Available online at www.sciencedirect.com
ScienceDirect
International Journal of Hydrogen Energy 31 (2006) 2310–2328
International Journal of HYDROGEN ENERGY
www.elsevier.com/locate/ijhydene

A wide range modeling study of NO_x formation and nitrogen chemistry in hydrogen combustion

A. Frassoldati*, T. Faravelli, E. Ranzi

CMIC Dipartimento di Chimica, Materiali e Ingegneria Chimica, Politecnico di Milano, Piazza Leonardo da Vinci 32, 20133 Milano, Italy

Received 6 December 2005; received in revised form 2 February 2006; accepted 13 February 2006
Available online 3 April 2006

Abstract

The chemistry of nitrogen species and the formation of NO_x in hydrogen combustion are analyzed here on the basis of a large set of experimental measurements.

The detailed kinetic scheme of H_2/O_2 combustion was updated and upgraded using new kinetic and thermodynamic measurements, and was validated over a wide range of temperatures, pressures and equivalence ratios. The mechanism's performance at high pressures was greatly improved in particular by adopting higher rate parameters for the $H + OH + M = H_2O$ reaction.

The NO_x sub-mechanism was further validated and updated. The kinetic parameters of the $NO_2 + H_2 = HONO + H$ and $N_2H_2 + NO = N_2O + NH_2$ reactions were updated in order to improve model predictions in specific conditions.

Sensitivity analyses were carried out to determine which reactions dominate the H_2/O_2 and H_2/NO_x systems at particular operating conditions.

Good overall agreement was observed between the model and the wide range of experiments simulated.

Keywords: Hydrogen kinetics; Combustion modeling; NO_x formation; Flame speed; Ignition delay; Hydrogen flames

1. Introduction

Hydrogen–oxygen and hydrogen–air systems can be used for many different applications including energy conversion and rocket propulsion. They also have relevance with regard to safety issues associated with planning for a possible future hydrogen economy [1]. The advantage of burning hydrogen from an environmental point of view is that it does not produce the greenhouse gas CO_2 or any of several other pollutant species, including CO, unburned hydrocarbons, PAH and soot. It therefore offers an opportunity to focus on the chemistry of NO_x formation and nitrogen compounds oxidation. However, until other uses for hydrogen are developed, there is still the need to increase efficiency and reduce pollutant emissions from stationary and mobile sources.

Even though the chemistry of hydrogen–oxygen combustion is better known than that of other combustion systems, research into the kinetics of hydrogen–oxygen systems still continues to achieve better accuracy [2]. Of course, the hydrogen oxidation mechanism lies at the core of all the combustion systems, a fact which provides additional motivation to accurately determine its reaction rate parameters. Such considerations are driving research aimed at a greater understanding of the kinetic mechanism. A large body of experimental measurements and kinetic studies has become available in

* Corresponding author.
E-mail address: alessio.frassoldati@polimi.it (A. Frassoldati).

0360-3199/$30.00
doi:10.1016/j.ijhydene.2006.02.014

recent years. For this reason, this paper initially focuses on the upgrading of the H_2/O_2 kinetic mechanism and then analyzes the chemistry of NO_x formation in these systems.

Recently, both Ó Conaire et al. [3] and Li et al. [4] discussed and upgraded their H_2/O_2 system kinetics on the basis of the work of Mueller et al. [5].

In fact, they extended the previous validation work to include different types of experiments and operating conditions in addition to flow reactors. The existence of recently revised thermodynamic data as well as new experimental high pressure experimental data justifies the revision, upgrading and complete validation of this kinetic model.

Ströhle and Myhrvold [6] tested the same mechanisms against experimental measurements for hydrogen combustion in lean conditions and at elevated pressures.

NO_x emissions from hydrocarbon combustion are the result of thermal and prompt mechanisms. In hydrogen flames, the prompt mechanism is not present but the high temperatures can promote high thermal NO_x production.

Hydrogen addition to hydrocarbon flames increases the flame temperatures and extends the flammability limits of the mixtures. NO_x formation can be minimized by reducing combustion temperature through carefully designed combustors.

The effect of H_2 addition on NO_x emissions from ultra low-NO_x burners was experimentally investigated by Athens et al. [7]. They observed that when pure hydrogen is burnt, NO_x emissions are very similar to those from pure natural gas, while a maximum is reached at about 70% H_2. The NO_x emissions increase up to the point when the increase caused by the thermal mechanism is balanced out by the decline of the prompt mechanism. At higher H_2 addition levels, the total NO_x emissions start to decrease. In contrast, NO_x emissions with conventional burners always increase as the hydrogen content increases. This effect is mainly due to the reduction of the thermal mechanism in ultra low-NO_x burners.

The general mechanism of nitrogen chemistry [8,9], coupled with the upgraded H_2–O_2 mechanism, is systematically compared against a wide range of experimental data, relating not only to NO_x formation in H_2 flames, but also laminar flame speeds, shock tube ignition delays, flow and stirred reactors. PREMIX and OPPDIF Sandia codes [10,11] are used for flame simulations, and multicomponent diffusion and thermal diffusion (the Soret effect) are always included since they are important in hydrogen combustion. We used the standard CHEMKIN transport package [12]. DSMOKE code is used to solve the equation systems of shock tube and ideal reactors [13].

2. Upgrading of the H_2/O_2 mechanism

Miller et al. [2] give a very interesting history of the kinetic modeling of hydrogen–oxygen systems starting with the pioneering kinetic study made by Semenov [14]. The key reactions of this system are discussed from both an experimental and theoretical point of view, with particular emphasis on the reactions between H and O_2.

The revised and upgraded H_2/O_2 reaction mechanism is reported in Table 1 and consists of 20 reversible reactions. The thermochemical data are summarized in Table 2. Reverse rate constants are calculated using the forward rate and equilibrium constants. All thermodynamic and transport properties are taken from the CHEMKIN Thermodynamic Database [15], with the exception of the enthalpy of OH and HO_2 formation.

In fact, these properties were recently revised following the theoretical and experimental recommendations made by Ruscic et al. [16] as the enthalpy of OH radical formation at 298 K is 8.91 kcal/mol, which is in excellent agreement with the experimental evaluation of Herbon et al. [17]. Moreover, Hills and Howard [18] propose a value of 3.0 kcal/mol for the enthalpy of HO_2 radical formation, in agreement with Ramond et al. [19].

As already mentioned, both Ó Conaire et al. [3] and Li et al. [4] modified the kinetics and also the thermodynamic data of the H_2–O_2 mechanism. While Ó Conaire et al. [3] used the previously quoted thermodynamic properties, Li et al. [4] adopted a slightly different value for HO_2. Both these mechanisms consist of 19 reversible reactions. Two further kinetic schemes, from Marinov et al. [20] and Del Alamo et al. [1], respectively, were also investigated in order to better complete this kinetic investigation. These mechanisms, which are not completely independent, differ significantly with regard to several rate parameters.

As already discussed elsewhere [21,22], a few kinetic modifications were applied to the original mechanism of Ranzi et al. [23].

The first modification refers to the reaction $H+OH+M = H_2O + M$ whose frequency factor was increased by a factor of 2. This modification was suggested by Ó Conaire et al. [3] and was also introduced by Davis et al. [24]. This reaction is primarily significant for laminar flame speed propagation at high pressure, while it is less sensitive under flow reactor and shock tube conditions. Similarly, there is a very marginal impact on hydrocarbon fuel combustion. The Chaperon efficiencies

Table 1
H_2/O_2 mechanism with rate coefficients in the form $k = A \cdot T^n \cdot \exp(-E_a/RT)$

	Reaction	A	n	E_a	Source
1	$H + O_2 = OH + O$	2.21E + 11	0	16 650	[81]
2	$O + H_2 = OH + H$	4.33E + 10	0	10 000	[82]
3	$H + O_2 + [M] = HO_2 + [M]$	7.00E + 11	−0.8	0	[83]
	Low pressure limit:	4.65E + 09	0.4	0	[26]
	Troe parameters: 0.5 1E − 30 1E + 30				
	Enhanced third-body efficiencies:				
	$H_2O = 18.0$ $H_2 = 2.5$ $N_2 = 1.26$ $O_2 = 0$ $Ar = 0.8$ $He = 0.8$ $CO = 2.11$ $CO_2 = 2.4$				
	$H + O_2 + O_2 = HO_2 + O_2$	8.90E + 08	0	−2822	[84]
4	$OH + HO_2 = H_2O + O_2$	5.00E + 10	0	1000	[85]
5	$H + HO_2 = OH + OH$	2.50E + 11	0	1900	[85]
6	$O + HO_2 = O_2 + OH$	3.25E + 10	0	0	[86]
7	$OH + OH = O + H_2O$	7.36E + 09	0	1100	[82]
8	$H_2 + [M] = H + H + [M]$	2.23E + 11	0	96 081	[87]
	Enhanced third-body efficiencies:				
	$H_2O = 12.0$ $H_2 = 2.5$ $O_2 = 0$ $CO = 1.9$ $CO_2 = 3.8$ $Ar = 0.5$ $He = 0.5$				
9	$O_2 + [M] = O + O + [M]$	1.55E + 11	0	115 120	[82]
	Enhanced third-body efficiencies:				
	$H_2O = 12.0$ $H_2 = 2.5$ $O_2 = 0$ $CO = 1.9$ $CO_2 = 3.8$ $Ar = 0.2$ $He = 0.2$				
10	$H + OH + [M] = H_2O + [M]$	4.50E + 16	−2	0	[88] ×2
	Enhanced third-body efficiencies: $H_2O = 16.0$ $H_2 = 2.0$ $CO_2 = 1.9$				
11	$H + HO_2 = H_2 + O_2$	2.50E + 10	0	700	[87]
12	$HO_2 + HO_2 = H_2O_2 + O_2$	2.11E + 09	0	0	[89]
13	$OH + OH + [M] = H_2O_2 + [M]$	7.40E + 10	−0.37	0	[90]
	Low pressure limit:	2.30E + 12	−0.9	−1700	
	Troe parameters: 0.7346 94.00 1756 5182				
	Enhanced third-body efficiencies:				
	$H_2O = 6.0$ $H_2 = 2.$ $CO = 1.5$ $CO_2 = 2.0$ $CH_4 = 2.0$ $C_2H_6 = 3.0$ $Ar = 0.7$ $He = 0.7$				
14	$O + OH + [M] = HO_2 + [M]$	1.00E + 10	0	0	[1]
15	$H + H_2O = H_2 + OH$	4.00E + 07	1	19 000	[84]
16	$H_2O_2 + H = H_2O + OH$	2.41E + 13	0	3970	[88]
17	$H_2O_2 + H = H_2 + HO_2$	6.03E + 13	0	7950	[88]
18	$HO_2 + H_2O \rightarrow H_2O_2 + OH$	5.39E + 05	2	28 780	[84]
19	$OH + H_2O_2 \rightarrow H_2O + HO_2$	3.20E + 05	2	−4170	[84]
20	$O + H_2O_2 \rightarrow OH + HO_2$	1.08E + 06	2	−1657	[84]

A units: $mol^{-1}\,s\,K$; E_a units: cal/mol.

Table 2
ΔH_f (298.15 K), S (298.15 K), and Cp (T) for species considered in the H_2/O_2 reaction mechanism

Species	ΔH_f	S	Cp (300 K)	Cp (1000 K)	Cp (2000 K)
N_2	0.0	45.816	6.949	7.830	8.601
H_2	0.0	31.256	6.902	7.209	8.183
O_2	0.0	49.050	7.010	8.350	9.032
H_2O	−57.80	45.154	7.999	9.875	12.224
H_2O_2	−32.53	55.725	10.416	15.213	17.878
OH	8.91	43.978	6.947	7.341	8.213
H	52.099	27.422	4.968	4.968	4.968
O	59.56	38.500	5.232	4.999	4.976
HO_2	3.000	54.809	8.349	11.380	13.321

Units are cal/mol/K for S and Cp, and kcal/mol for ΔH_f.

of the bath gases were also slightly modified to improve the agreement with the whole set of experimental measurements.

Of course, the H and O_2 reactions and, for the most part, their relative rates govern the reactivity and the behavior of the system. Special attention was devoted to the reaction $H + O_2 + M = HO_2 + M$, particularly its fall-off kinetics and third-body efficiencies. Del Alamo et al. [1] and Li et al. [4] modified this reaction, too.

As already discussed by Saxena and Williams [25], on the basis of recent calculations of potential energy surfaces, the reaction $H_2 + O_2 = 2OH$ is highly unlikely and was therefore removed from the mechanism. This step only slightly influences the predicted induction times and the reactivity of the system.

For very high pressure applications, in order to adequately describe the fall off behavior of the reaction $H + O_2 + M = HO_2 + M$, the high pressure limit was added to the mechanism following Troe's [26] parameters and fall-off recommendations.

3. Validation of the H_2/O_2 kinetic scheme

This upgraded kinetic scheme was systematically compared to a wide range of experimental data. The whole set of data, as reported in Table 3, includes laminar flame speeds, shock tube ignition delay times, flow reactors and burner-stabilized flames. The complete detail of these data and model comparisons is reported in Appendix A. Some relevant results are reported here and discussed in order to analyze the effect of the kinetic modifications as well to present some interesting features.

The correct prediction of the p–T explosion limits is critical for safety reasons, particularly in the design of premixed systems. The explosion diagram of a stoichiometric H_2/O_2 mixture is discussed by Lewis and Von Elbe [27] and by Maas and Warnatz [28]. The *first ignition limit* is strongly dependent on vessel size and the nature of the surface, which influence the overall chain termination reactions. The *second ignition limit*, however, is kinetically ruled by the competition between the chain branching reaction $H + O_2 = OH + O$ and the third-body reaction $H + O_2 + M = HO_2 + M$ which produces the more stable HO_2 radical. The second limit is thus also strongly dependent on the Chaperon efficiencies. The high pressure or *third explosion limit* is sensitive to the heat losses from the wall.

As already noted by various authors [28], the gas phase reactions alone are not sufficient to characterize the behavior of the system, especially for the first limit which is heavily influenced by heterogeneous radical recombination. The third limit, on the other hand, is influenced by the heat flux at the wall that controls the effective temperature.

For the sake of simplicity, this closed system is assumed as a simple batch-reactor with heat exchange. Fig. 1 compares model predictions and experimental data. Note that the heat transfer coefficient was used as a parameter to fit the third limit. Model predictions with the external heat transfer coefficient increased by one order of magnitude are also reported. As expected, the effect on the second limit is almost negligible. A more complete simulation of this system was already reported and discussed by Maas and Warnatz [28].

Fig. 2 compares measurements and predictions of the second ignition limit with different kinetic mechanisms,

Table 3
Experimental measurements on hydrogen systems studied in this paper

Experiment	Mixture	Temperature (K)	Φ	Pressure (atm)	Figures	Source
P–T explosion limits	H_2/O_2	650–900	1.0	0–1	1, 2	[28–32]
Plug flow reactor	$H_2/O_2/N_2$	800–935	1.0	0.3–15.7	A1	[5]
Ignition delay times	H_2/O_2/Ar	1000–2900	0.25–1	1	A2a	[72]
	$H_2/O_2/N_2$	950–1350	1	2–2.5	A2b	[73,74]
	H_2/O_2/Ar	1250–1800	0.5	3	A3a	[75]
	H_2/O_2/Ar	950–1050	2	1	A3b	[76]
	H_2/air	830–1430	1	1	A4a	[77]
	H_2/O_2/Ar	1150–2000	1	33–64	A4b	[78]
	H_2/air/H_2O	900–1300	0.42	3.95	3	[37]
Premixed flame	H_2/O_2/Ar	570–1170	1.91	0.0467	A5	[79]
Flame speeds	H_2/air	300	0–5	1–20	4	[38–44]
	H_2/O_2/Ar–He					
	H_2/CO/CO_2–air	298	0.6–2.4	1	A6	[80]
Ignition in a counterflow configuration	H_2/Air/H_2O	300–1100	0–∞	1	5	[45]

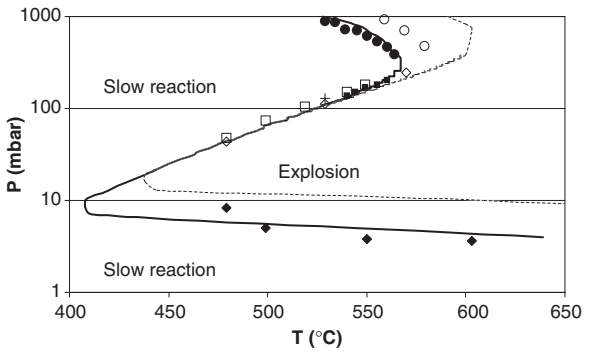

Fig. 1. Ignition limits in the H_2–O_2 system. Comparison between experimental measurements (symbols) and simulation (continuous line). Dotted line: simulation obtained increasing the external heat transfer coefficient by a factor of 10. Experimental results: diamonds: silica vessel (filled) [29], KCl-coated vessel (empty) [30]; crosses: clean pyrex vessel [30]; circles: heavily KCl-coated vessel (empty), KCl-coated vessel (filled) [31]; squares: thinly KCl-coated vessels (filled) [31], B_2O_3-coated vessel (empty) [32].

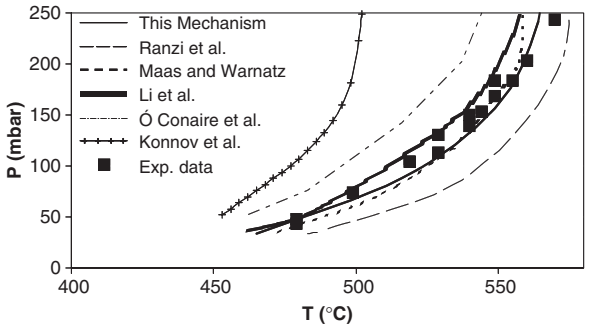

Fig. 2. Second ignition limit in the H_2–O_2 system. Comparison between experimental measurements (see Fig. 1) and the present model (continuous line), the previous mechanism [23] (long-dashed line), Maas and Warnatz mechanism [28] (dashed line), Ó Conaire mechanism [3] (dot–dashed line), Li mechanism [4] (gray line) and Konnov mechanism [33] (line with crosses).

always with the same heat transfer coefficient. The improvement obtained, as a result of the refinement of the previous mechanism [30], is clear. The agreement is also satisfactory when the mechanisms of Li et al. [4] and Maas and Warnatz [27] are used, while the mechanism of Ó Conaire et al. [3] and particularly Konnov [33] overestimate the reactivity. Good agreement is also obtained using GRI 3.0 [34], San Diego mechanism [1], and the mechanism of Skreiberg et al. [35] (not shown).

Mueller et al. [5] studied the reactivity of a dilute H_2/O_2 mixture in a flow reactor at pressures ranging from 0.3 to 15.7 atm and temperatures from 880 to 935 K. At 3.44 atm, the system exhibits an induction period followed by rapid chain-explosive oxidation, while both at lower and at higher pressure, the H_2 consumption is a slow, stable process: these data confirm the correct model predictions of the competition between the two $H + O_2$ reactions under these conditions too.

These same reactions, and the Chaperon efficiency, are very sensitive in the predictions of ignition delay times. Shock tube induction times from the literature were accurately catalogued by Schultz and Shepherd [36] for hydrogen, ethylene and propane. Ignition delays in very different temperature and pressure conditions have indeed been successfully simulated and contribute to the validation of the mechanism. The recent data reported by Wang et al. [37] are reported in Fig. 3 to provide a sample of these comparisons. Once again the sensitivity analysis confirms the importance of the three body reaction between H and O_2. The effect of different amounts of H_2O added to a H_2–air mixture at 1200 K is reasonably predicted by the kinetic model.

The ability to model laminar flames is not only related to the kinetic scheme but also to the transport properties. A collection of several experimental hydrogen flames was recently summarized by Ó Conaire et al. [3] and Li et al. [4]. Fig. 4a shows the good comparisons between experimental and predicted flame speed of several H_2/air systems at 1 atm as a function of the equivalence ratio. Predictions compare very well with experimental measurements across the whole range of equivalence ratios. The effect of the bath gas is clear from the data of Kwon and Faeth [44] where N_2 is replaced by He or Ar. Model predictions properly account for the differences, which are mainly due to the flame temperatures, Chaperon efficiencies and transport properties. The trend of the flame speed with the pressure is well reflected by the model, at two levels of He dilution [43] (Fig. 4b). The original mechanism [23] overestimates the flame speeds at high pressure up to about 15–20%. As already mentioned, the increased rate constant of reaction $H + OH + M = H_2O + M$ allows closer agreement with the experimental data.

The last comparison between model predictions and experimental data refers to the very recent data of Seiser and Seshadri [45]. They studied the effect of water addition on the autoignition temperature of hydrogen flames in a counterflow configuration. Fig. 5 shows that the addition of water makes the flame harder to ignite. The autoignition temperature is extremely sensitive to the third-body efficiency of H_2O in the $H+O_2+M=HO_2+M$ reaction.

As already mentioned, the complete set of model predictions and comparisons with experimental data for the H_2–O_2 systems is reported in Appendix A.

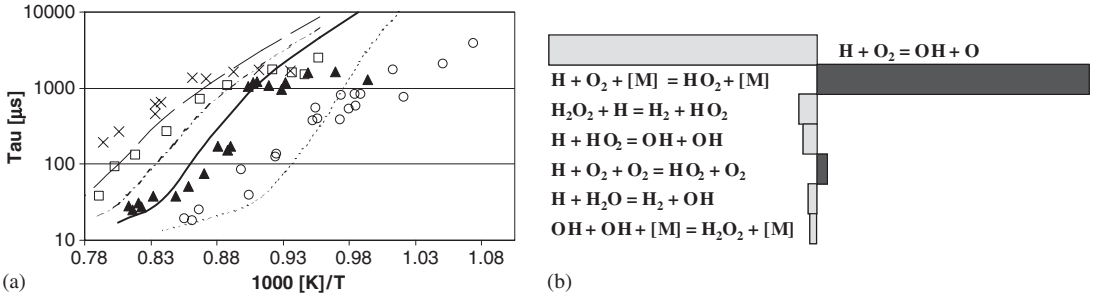

Fig. 3. (a) Comparison between predicted ignition delay times and experimental data [37] in a H_2–air mixture with different amounts of steam at 0.4 Mpa. Lines represent model predictions, symbols are experimental measurements. Circles and dotted line: 0% H_2O, triangles and continuous line: 15% H_2O, squares and dash–dotted line: 25% H_2O, crosses and long-dashed line: 40% H_2O. (b) Sensitivity coefficients for H_2 at early stage of ignition at $T = 1200$ K and 25% H_2O. Dark bars correspond to positive sensitivity coefficients

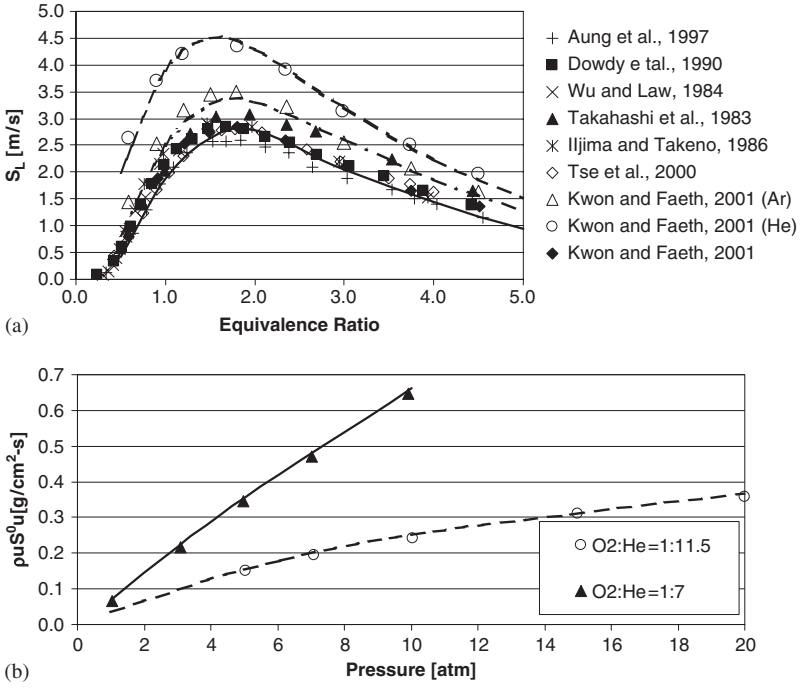

Fig. 4. (a) Comparison between measured [38–44] and predicted H_2 flame speeds at 1 atm and 298 K. (b) Effect of pressure on H_2 mass burning velocity for H_2/O_2/He at two levels of dilution in He. Experimental data from Tse et al. [43].

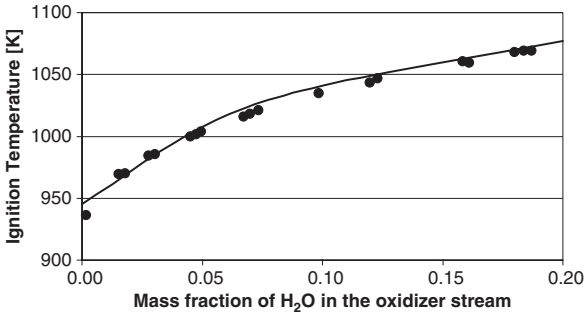

Fig. 5. The temperature of the oxidizer stream at autoignition of nonpremixed hydrogen flames, as a function of the mass fraction of water vapor in the oxidizer stream. Symbols represent measurements [45] and the lines are results of numerical calculation.

4. Chemical kinetics of NO_x in hydrogen flames

In previous papers [8,9], the chemistry of nitrogen components and principally their interactions with hydrocarbon fuels across the whole range of temperature conditions were discussed, and a detailed kinetic scheme was presented and validated. This kinetic scheme, coupled with the upgraded H_2–O_2 scheme, is further discussed here and validated by comparison with various new experimental data relating mainly to hydrogen combustion and hydrogen flames.

Table 4
Experimental measurements on hydrogen/NO_x systems studied in this paper

Experiment	Mixture	Temperature (K)	Φ	Pressure (atm)	Figures	Source
Counterflow flame	H_2–N_2–O_2–He/air	300–2100	0–∞	1	6	[46]
Premixed flame	H_2–air	~ 1200	1.5	0.103	7a	[50]
Premixed flame	H_2–N_2–O_2	300	0.71	1	7b	[51]
Stirred reactor	H_2–air	1400–1600	0.6	1	8	[52]
Ignition delay times	H_2/air + NO	800–1200	1	1	9a, 9b	[53]
Ignition delay times	H_2/air + NO_2	800–1200	1	1–4	11	[54]
Ignition delay times	N_2O/Ar	1000–2500	—	1–14	12	[55]
Flame speeds	H_2/N_2O	333	0.25–4	0.09	13	[61]
Premixed H_2/N_2O/Ar flames (NH_3-doped)	H_2/N_2O/Ar + NH_3	300	~ 1.08	0.039	14	[63]
Ammonia chemistry in a flow reactor	$NO/NH_3/O_2/N_2 + H_2$	1273	—	1	15	[66]
Ignition delay times	$NH_3/O_2/H_2$/Ar	1250–2000	—	5.7–8	16a	[67]
Ignition delay times	NH_3/NO/Ar	1670–2500	—	1.3	16b	[68]
Flame speeds	NH_3/O_2	298	0–2.5	1	17	[69–71]

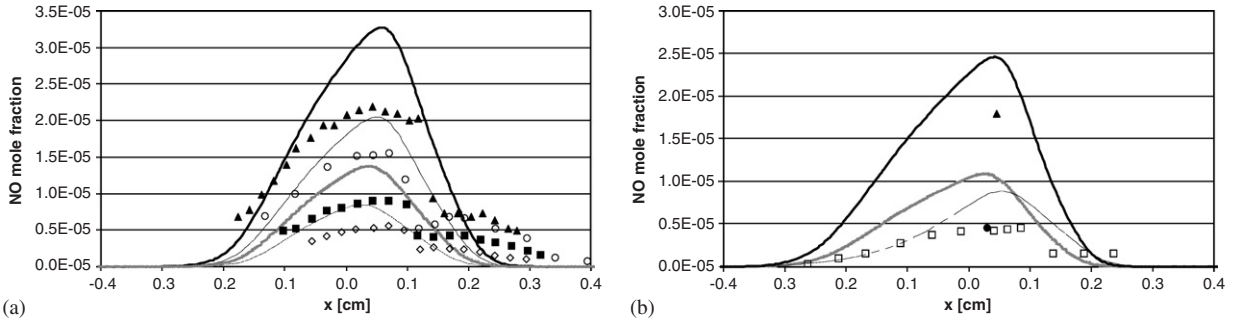

Fig. 6. (a) NO profiles in H_2/air diffusion flames at different fuel dilution with N_2. Triangles and thick line 55% N_2; circles and thin line 60% N_2; squares and gray line 65 % N_2; diamonds and dashed line 70% N_2 in fuel stream. (b) NO profiles in H_2/air diffusion flames at different fuel dilution with He. Triangle and thick line 50% He; circle and gray line 60% He in fuel stream. Squares and dashed line: partially premixed flame 30% H_2, 5.5% O_2 and 64.5% N_2 in fuel stream. Symbols: experiments [46]; lines: modeling.

Of course, the greatest interest lies in the proper prediction of NO_x formation in H_2 combustion. However, the interactions between nitrogen compounds and hydrogen oxidation mechanism are also a critical feature of this reacting system. Table 4 summarizes the experimental data used for this validation of the kinetic model.

4.1. NO_x formation in counterflow diffusion flames

Rørtveit et al. [46] investigated the effect of diluents on NO_x formation in H_2 counterflow diffusion flames at a constant strain rate of 100 s^{-1}. The oxidizer is air and the hydrogen at the fuel inlet is diluted with different amounts of N_2. A standard model for radiative heat loss from H_2O was applied in the simulation, resulting in a reduction of less than 5 K in the flame temperatures. Calculated flame temperatures compare well with the experimental measurements and range between 1812 and 2122 K.

Rørtveit et al. [46] discussed the uncertainties of these experiments. The predicted NO shows a temperature dependency that is weaker than the experimental one. Their conclusion was that at the higher temperatures, NO was removed by chemical reactions with H-atoms on the quartz wall of the probe. Moreover, a significant catalytic effect (at 2000–2200 K) is peculiar to H_2 flames because of the very high concentrations of H atoms. The experimental uncertainties of [NO] are within 10%. The sudden change of the measured NO fraction close to the maximum temperature was due to the attachment of the flame to the probe.

Dilution reduces the flame temperature and thus the thermal mechanism of NO_x formation (Fig. 6a). At high dilutions, the thermal mechanism is almost suppressed

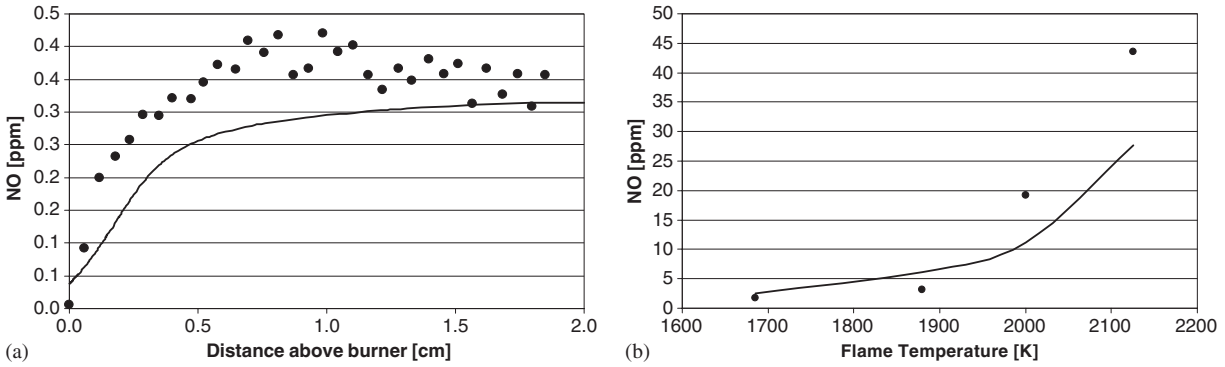

Fig. 7. (a) NO profile in a premixed H_2/air flame at $P = 78$ torr. Symbols: experiment [50]; lines: modeling. (b) Flames of H_2/O_2 mixtures at equivalence ratio $\Phi \cong 0.71$ and different dilution with N_2. Measured [51] (symbols) and calculated (line) [NO] at 2 cm downstream of the flame front.

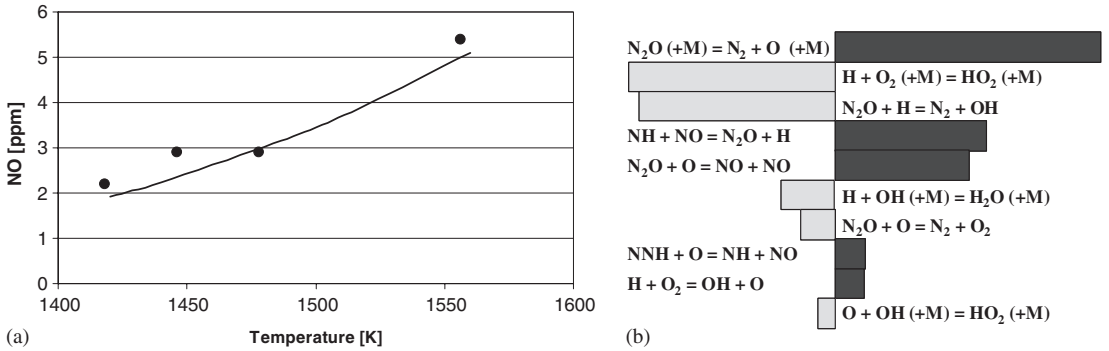

Fig. 8. (a) NO formation in H_2/air mixtures in a stirred reactor. Symbols: experiment [52]; lines: modeling. (b) Sensitivity coefficients for [NO] in a stirred reactor at $T = 1500$ K and $\Phi = 0.6$. Dark bars correspond to positive sensitivity coefficients.

and NO_x formation mainly occurs through NNH and N_2O mechanisms. Both the effects of He dilution and the effect of the partial O_2 premixing are properly predicted by the model, as shown in Fig. 6b. The deviations in NO predictions at higher temperatures can be at least partially attributed to the catalytic removal of NO on the quartz probe. Moreover, Park et al. [47] modeled this flame and found similar results.

4.2. Burner-stabilized flames: H_2/air flames at low P and moderate T ($\sim$ 1200 K)

Two main reaction paths forming NO_x are relevant in H_2 combustion: thermal NO and the nitrous oxide mechanism (N_2O). The NNH mechanism [48] is always important at low temperatures [49], while it is relevant only at low residence times for rich mixtures at high temperatures. The burner-stabilized H_2/air flames at low pressure, and moderate temperatures ($\sim$ 1200 K) support and confirm this information [50]. Fig. 7a shows the comparison between measurements and model predictions obtained with the measured temperature profile [50]. Fig. 7b shows that NO predictions agree well with the experimental measurements in premixed flames at higher temperatures too [51].

4.3. H_2/Air mixtures in a stirred reactor

Xie et al. [52] studied the combustion of H_2/Air mixtures with $\Phi = 0.6$ in a stirred reactor at temperatures between 1400 and 1550 K. Fig. 8a reports the comparison between the experimental and predicted NO formation in the different conditions, and Fig. 8b shows the corresponding sensitivity analysis. This analysis highlights the relevant role of the N_2O mechanism and the competition between the different paths leading to the formation of N_2 and NO for the reactions of N_2O with H and O.

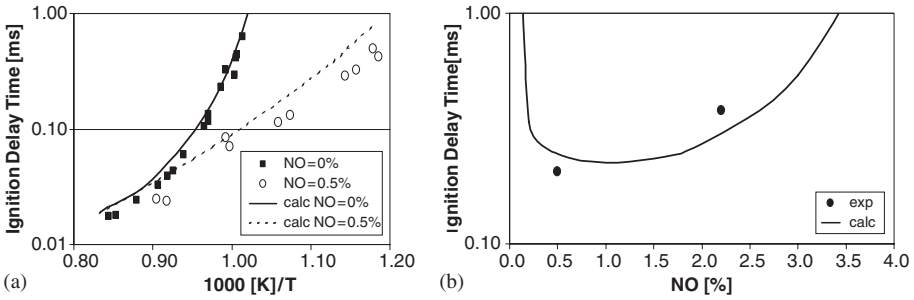

Fig. 9. (a) Ignition times for stoichiometric H_2–air mixtures both with and without added NO. (b) Ignition times for stoichiometric H_2–air mixtures at different NO concentration. Symbols represent measurements [53] and the lines numerical calculations.

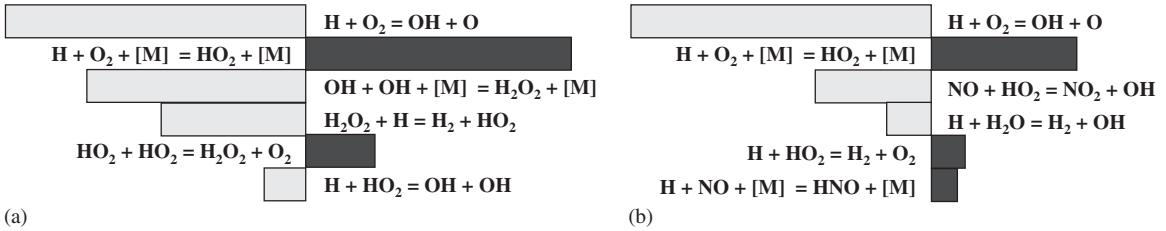

Fig. 10. Sensitivity coefficients for $[H_2]$ at conditions close to ignition for stoichiometric H_2–air mixture at 900 K and $P = 2$ atm: (a) without NO addition, (b) with 0.5% NO. Dark bars correspond to positive sensitivity coefficients.

4.4. NO addition to H_2–O_2 systems: effect on ignition delay times

Laster and Sojka [53] studied the effect of NO addition on the ignition delay times of H_2–air mixtures. NO addition significantly reduces the ignition delays. This accelerating effect is of particular interest since NO_x are commonly present in vitiated airstreams. Fig. 9a compares model predictions with the experimental measurements of ignition delay time of stoichiometric H_2–air mixtures both with and without added NO. Fig. 9b shows that the model is also able to predict the dependence of ignition delay on NO concentration.

Fig. 10 shows the sensitivity coefficients for $[H_2]$ at 900 K and conditions as in Fig. 9, for H_2–air mixtures with and without NO added. In the earliest stage of the simulation, the ignition delay time is very sensitive to the reaction $H_2 + O_2 = OH + OH$, which creates the radical pool responsible for the successive chain branching process. The presence of NO in the systems balances the chain terminating step $H + O_2$ because HO_2 is rapidly transformed to the reactive OH radical. The sensitivity analysis confirms the role of nitrogen chemistry in the low temperature regime, as already discussed by Faravelli et al. [8]. Fig. 11 shows the effect of NO_2 addition on the ignition delay times of H_2–air mixtures at

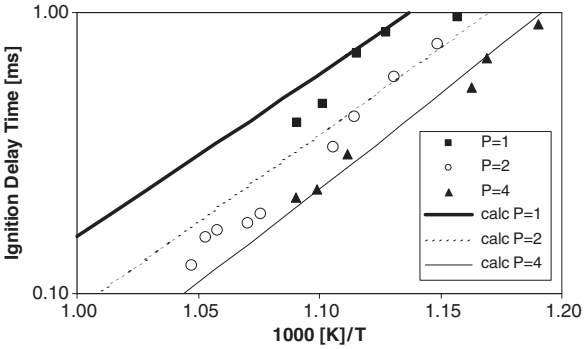

Fig. 11. Ignition times for stoichiometric H_2–air mixtures in the presence of 3.56% of NO_2 at different pressures (1–4 atm). Symbols are the experimental measurements [54] and lines represent model results.

different pressures. The ignition delay is strongly influenced by the $NO_2 + H_2 = HONO + H$ reaction. In order to improve the model, its rate parameters were updated following the indications of Slack and Grillo [54].

Ignition delays of pure N_2O were determined behind reflected shock waves at 1 atm and higher pressure for N_2O/Ar mixtures by Borisov and Skachkov [55]. The sensitivity analysis shown in Fig. 12b highlights the role of the dissociation reaction of N_2O, which is

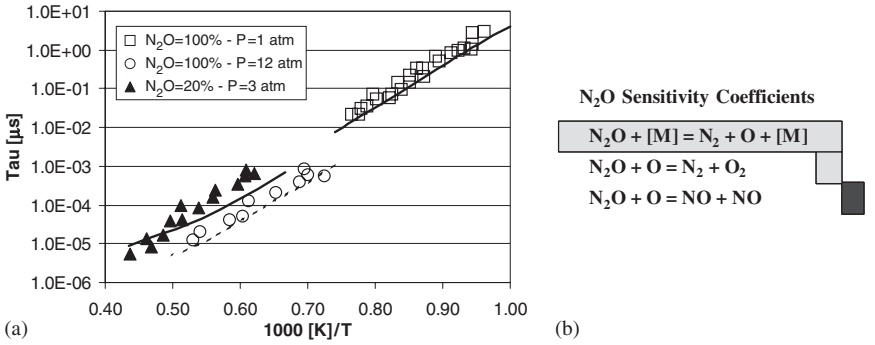

Fig. 12. (a) Ignition times of nitrous oxide [55]. Squares: 100% N_2O and 1 atm. triangles: 20% N_2O, 80% Ar and 2.5–3.5 atm; circles: 20% N_2O, 80% Ar and 10–14 atm. (b) Sensitivity coefficients for [N_2O] at 1200 K and 1 atm. Dark bars correspond to positive sensitivity coefficients.

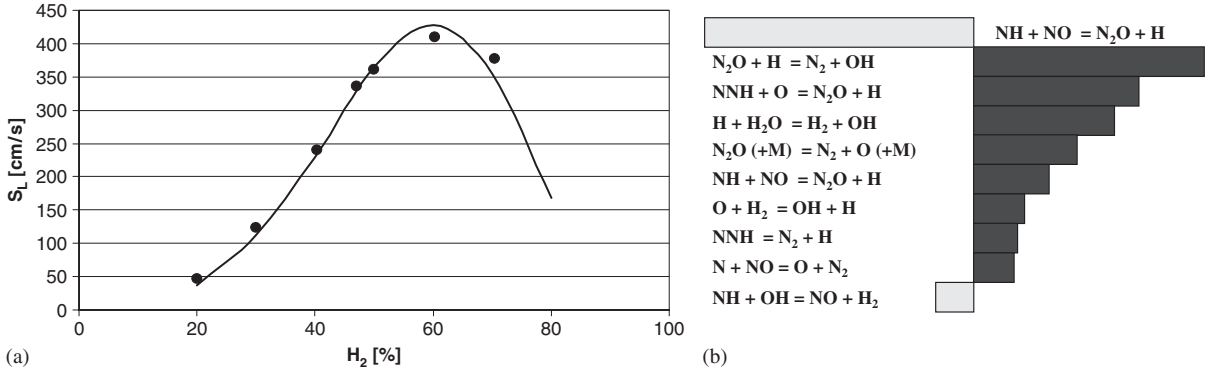

Fig. 13. (a) Laminar flame speeds in H_2/N_2O mixtures at $P = 70$ torr and $T = 333.15$ K. Symbols represent experimental data [61]. (b) Sensitivity coefficients for flame speed of Fig. 4b, $[H_2] = 60\%$. Dark bars indicate positive coefficients.

also responsible of NO_x formation via the nitrous oxide mechanism in combustion systems. These experimental data were already successfully modeled by Konnov [56] who adopted the reaction rate parameters suggested by Rohrig et al. [57] for the dissociation of N_2O and were close to the values used in the mechanism of Li and Williams [58]. We use the reaction rate parameters suggested by Johnsson et al. [59] and employed in the mechanisms of Bendtsen et al. [60].

4.5. Laminar flame speeds of H_2/N_2O mixtures

Fig. 13 shows the comparison between measurements and model results of freely propagating H_2/N_2O flames as a function of the equivalent ratio. The good agreement in the flame speed predictions shows that the N_2O chemistry too is well accounted for in the kinetic scheme.

Fig. 13b shows the corresponding sensitivity analysis. It is worth noting the competition between the three different channels of the reaction $N_2O + H$. The ones producing the reactive O and OH radicals exhibit positive coefficients, while the formation of NH and NO reduces the reactivity of the system.

4.6. Role of NH_3 chemistry on NO_x emissions from combustion systems

Under favorable operating conditions, NH_3 selectively converts NO to N_2. This is used in practice in the thermal deNO_x process by adding ammonia, urea and similar compounds to flue gases to remove NO. The chemistry of NH_3–H_2 systems is thus relevant to the better understanding and optimization of the selective non-catalytic reduction (SNCR) technology.

Moreover, ammonia is a primary volatile product of organic nitrogen compounds in biomass fuels and can also be formed in significant amounts during coal pyrolysis. Due to the importance of ammonia as a source of fuel-NO, there is considerable interest in understanding

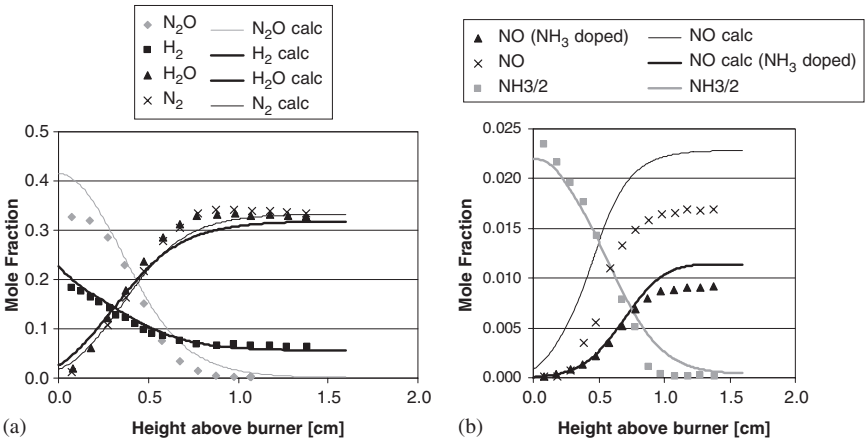

Fig. 14. Calculated (lines) and experimental (symbols) [63] species profiles in a 30 torr $H_2/N_2O/Ar$ flame: (a) neat flame, (b) NO profiles for the neat flame (crosses), NO (diamonds) and NH_3 (squares) profiles for the doped flame ($NH_3 = 4\%$).

the chemistry of ammonia in order to minimize NO formation. In fact, solid fuels are expected to make a large contribution to energy production in the near future. In addition to coal, various biomass fuels as well as household and industrial waste are now more widely used as energy sources. This introduces new challenges in pollution control and modeling. In most solid fuel fired systems, in fact, the oxidation of fuel-bound nitrogen constitutes the dominating source of nitrogen oxides. Solid fuels, such as coal, peat, most agricultural residues, etc., contain the order of 1% nitrogen [62]. HCN is the major nitrogen-containing species formed during the gasification of bituminous coal. In addition to HCN, significant amounts of NH_3 are released during the devolatilization of low-rank coals and biomasses [62]. The NH_3 is then converted to NO or N_2 depending on the local reaction conditions.

Furthermore, the use of the existing effective primary and secondary measures employed in pulverized-coal-burning equipments to control NO_x emissions may not be viable for fuels like biomass and waste. For instance, catalytic flue gas cleaning is prevented by trace components such as alkali metals which cause catalyst deactivation. Thus, it is clear that a better understanding of nitrogen chemistry in solid fuel fired systems would be helpful principally in improving primary NO_x control measures.

4.7. Premixed $H_2/N_2O/Ar$ flames (NH_3-doped)

Sausa et al. [63] studied low-pressure $H_2/N_2O/Ar$ flames, both pure and NH_3-doped, to further investigate the main NO formation mechanisms in flames and to evaluate the role of NH_3 in the reduction of NO to N_2. The addition of 4% NH_3 shifts the profiles away from the burner and reduces NO by about 45%. The experimental temperature profile is used in the modeling of this flame operated at $\Phi \cong 1.1$.

The satisfactory comparisons between the experimental measurements and model predictions are presented in Fig. 14. In order to improve model predictions the $N_2H_2 + NO = N_2O + NH_2$ reaction was modified by adopting the rate parameters suggested by Skreiberg et al. [35]. In fact, NO in the NH_3-flame is sensitive to the reaction between NH_2 and N_2O while the results in the undoped conditions are almost unaffected by this modification. NO concentration is slightly overpredicted, especially in the undoped flame. This deviation does not seem to be a systematic deviation of the kinetic model. It is not, in fact, fully consistent with other comparisons. This NO over-prediction can be attributed to the $NH + OH = NO + H_2$ reaction which is not present in all NO_x sub-mechanisms. For instance, the mechanisms of Skreiberg et al. [35], Bendtsen et al. [60], GRI mech [34] and Li and Williams [58] do not include this reaction, while it is taken into consideration in the mechanisms developed by Konnov [33], Dagaut et al. [64] and Klaus and Warnatz [65]. Interestingly, the modeling of this flame using the different kinetic schemes reveals that NH_3 profile is not satisfactorily predicted using the mechanism of Skreiberg et al. [35], Konnov [33] and Li and Williams [58], although NO profiles are in good agreement with measurements. Bendtsen et al.'s [60] mechanism, on the other hand, correctly predicts NH_3 but does not account for the NO reduction in the doped flame. This kinetic uncertainty seems to require not only a theoretical analysis of the $NH + OH = NO + H_2$ reaction but, even more

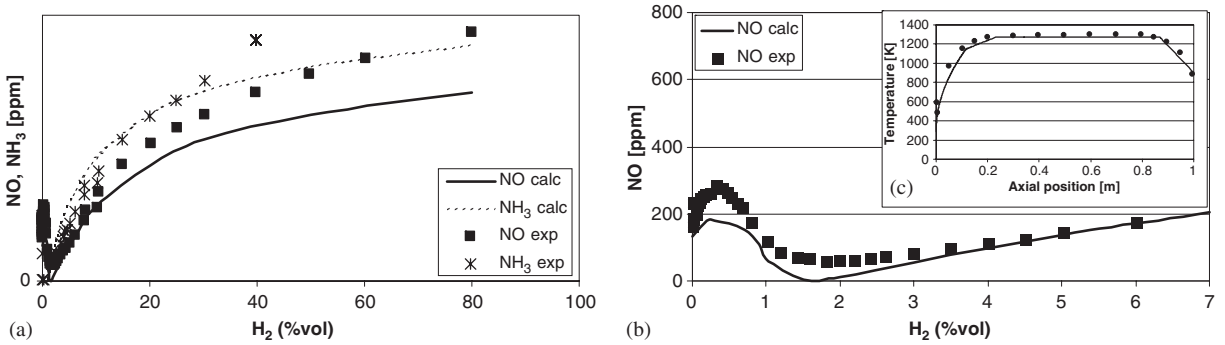

Fig. 15. (a) Calculated (lines) and experimental (symbols) [66]. NH_3 and NO at 1273 K as a function of the inlet H_2 concentration. Inlet composition: 1000 ppm of NO, 1000 ppm NH_3, 5000 ppm O_2, balance N_2. (b) Same conditions of Fig. 15a with an expanded x-axis to emphasize the low H_2 region. (c) Comparison between temperature measurements [66] and the temperature profile used in the calculations.

importantly, further experimental data. In fact in their modeling work, Sausa et al. [63] too observed some discrepancies mostly relating to a decay of predicted NO in the burned gas, which was attributed to a scarce reactivity of NH_3. In that analysis they also indicated experimental uncertainties with regard to the peak temperature.

4.8. Ammonia chemistry in a flow reactor

Hasegawa and Sato [66] studied the NH_3 oxidation under fuel-rich conditions and moderate temperatures in a flow reactor. These operating conditions are similar to the SCNR ones with different fuels (H_2, CO, CH_4). Their major interest was ammonia removal from a surrogate coal-gasification gas. Nonetheless, these experimental measurements provide further useful data for model validation. The reactants are mixed at room temperature and the temperature profile inside the reactor, after initial heating, is quasi isothermal in the central zone. Skreiberg et al. [35] have already verified and tuned their kinetic mechanism, and identified the major reaction paths responsible for NO reduction by NH_3 under these conditions. Moreover, they also found that the model was sensitive to the shape of temperature profile to a limited extent. On the basis of this fact, we simplified the description of temperature evolution inside the reactor by using a series of four variable temperature flow reactors. Fig. 15c shows the comparison between the measurements and the temperature profile used in the calculations.

Fig. 15 shows the conversions of NO and NH_3 inside the reactor as a function of the inlet hydrogen concentration. NO and NH_3 are reasonably predicted over the full range of conditions. Specifically, the trend of NO conversion at very low H_2 levels is well calculated, although NO is underestimated at low H_2. However, NO is underpredicted at high H_2. The most significant difference between these predictions and the results of Skreiberg et al. [35] relates to the relative concentrations of NO and NH_3. In the results obtained by Skreiberg et al. [35], the predicted profiles of the NO and NH_3 mole fraction are nearly identical over the full range of H_2 concentration, due to the fact that amine radicals react almost exclusively with NO. The enhanced NO conversion rate observed in the experiment is not predicted.

Sensitivity analysis reveals that both NH_3 and NO, are sensitive to the key abstraction reaction $NH_3 + H = NH_2 + H_2$ which is shifted towards NH_3 at high hydrogen levels, inhibiting the conversion of NH_3. The conversion of NH_3 produces the amine radicals responsible for the NO reduction due to the $NH_2 + NO = N_2 + H_2O$ and $NH_2 + NO = NNH + OH$ reactions. However, very small amounts of H_2 improve reactivity thus enhancing the radical pool, and H in particular, promoting the formation of NH_2 and the reduction of NO. The competition between the enhancing and inhibiting effect of H_2 accounts for the minimum of NO at about 2% of H_2 content.

4.9. Ignition times of NH_3–O_2–H_2–Ar mixtures

The effect of hydrogen addition on ammonia oxidation was studied in a shock tube device by Fujii et al. [67]. The comparison between experimental measurements and model results is summarized in Fig. 16.

As usual for combustion systems, the $H+O_2=OH+O$ reaction plays a relevant role when hydrogen is added

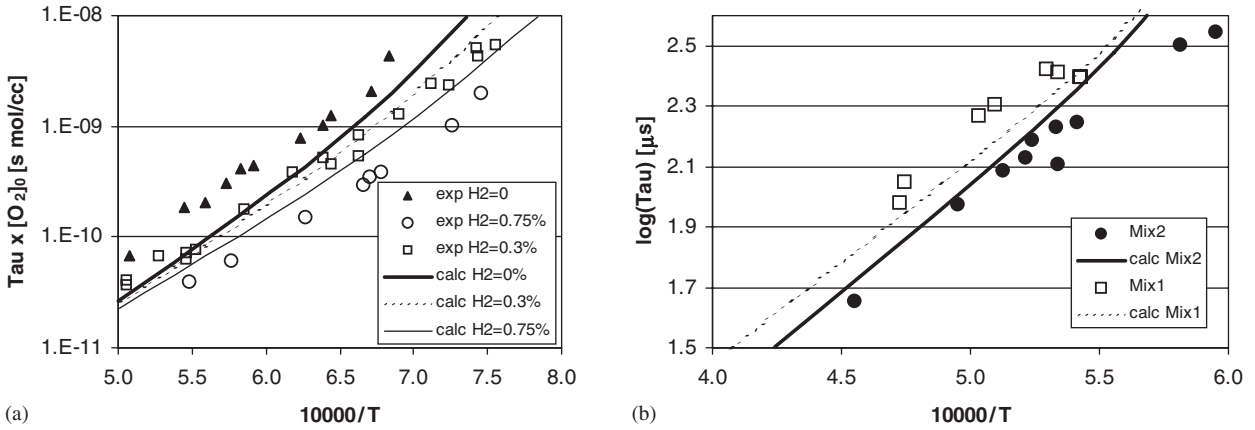

Fig. 16. (a) Ignition times of NH_3–O_2–H_2–Ar mixtures [67]. NH_3 and $O_2 = 0.05$, variable H_2, balance Ar. (b) Ignition delay times for NH_3–NO–Ar mixtures [68]. $NH_3 = 4\%$, $NO = 4\%$ (squares), 6% (circles), balance Ar.

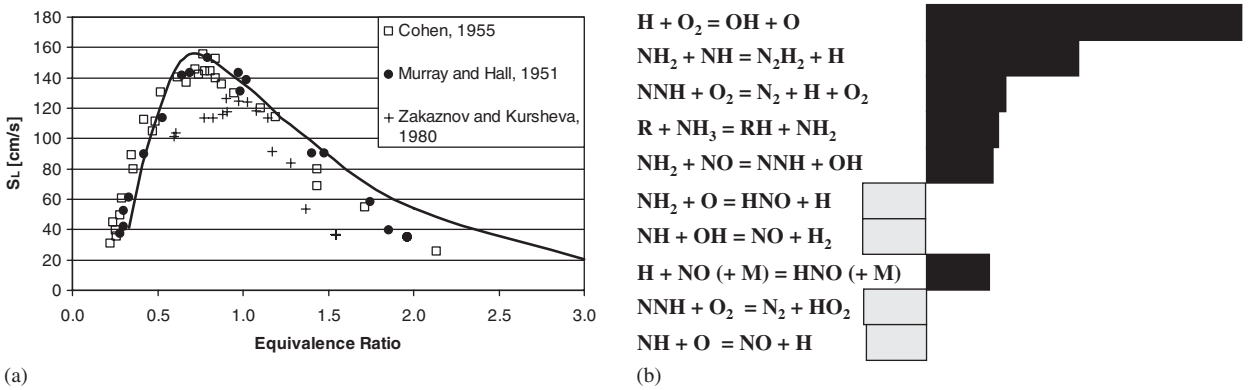

Fig. 17. (a) Laminar flame speeds in NH_3/O_2 mixtures at $P = 1$ atm and $T = 298$ K. Symbols represent experimental data [69–71]. (b) Sensitivity coefficients for flame speed of Fig. 4b, $[H_2] = 60\%$. Dark bars indicate positive coefficients.

to the system although the two following reactions also wield significant influence:

$$NH_2 + O_2 = H_2NO + O$$

$$H_2NO + M = HNO + H + M.$$

In fact, the final result of these two reactions is $NH_2 + O_2 = HNO + H + O$ and constitutes a degenerate branching path.

Shin et al. [68] studied different NH_3–NO–Ar systems at high temperatures. These data too contribute to the validation of the overall kinetic scheme. The replacement of O_2 with NO changes the reactions responsible for NH_3 ignition. In fact, for this NH_3–NO–Ar system, the ignition delay is governed by the competition between the $NH_2 + NO = NNH + OH$ and $NH_2 + NO = N_2 + H_2O$ reactions.

4.10. NH_3 flame speeds

This final example refers to freely propagating NH_3/O_2 flames in different conditions. Comparisons between measured and predicted flame speed are reported in Fig. 17. The good agreement confirms that the nitrogen chemistry relating to the modeling of flame speeds is also well reflected in the kinetic scheme.

The sensitivity analysis of this flame (Fig. 17b) once again confirms that it is the competition of parallel paths more than the absolute reaction rate that rules the reactivity of the system. Here, two different channels of $N_2O + H$ produce the reactive O and OH radicals, and then increase the flame speed, while the $N_2O + H = NH + NO$ reaction forms more stable species and reduces the reactivity.

5. Conclusions

The chemistry of nitrogen species and the formation of NO_x in hydrogen combustion were analyzed on the basis of a large set of experimental measurements and data relating to different devices. Two main results were obtained.

The detailed kinetic scheme of the H_2/O_2 submechanism was updated and upgraded on the basis of new measurements as well as new thermodynamic information.

The kinetic scheme of NO_x formation and nitrogen species interactions with the combustion environment was further validated. As already discussed, only two modifications were applied in respect of the previous kinetic scheme [8]. Firstly, the kinetic parameters of the $NO_2 + H_2 = HONO + H$ reaction were updated using the indications of Slack and Grillo [54].

Secondly, the $N_2H_2 + NO = N_2O + NH_2$ reaction was modified in order to improve model predictions in the N_2O/H_2 flame doped with NH_3.

It is important to stress that both these reactions are very sensitive in the conditions analyzed; nevertheless, these kinetic modifications have only a marginal impact in different reacting systems.

The proposed model was validated against the available data for H_2/NO_x systems including laminar flames, stirred and plug flow reactors and ignition delay times in shock tubes. The formation of NO in hydrogen flames as well as the effect of NO_x on the reactivity was discussed in detail on the basis of sensitivity analysis in order to emphasize the specific role of the reactions in different operating conditions. The relevant role of N_2O and NH_3 chemistry was also highlighted. The whole set of comparisons between experimental measurements and model strongly supports the reliability of the kinetic scheme.

Acknowledgment

This project was financially supported by MIUR (COFIN project 2003).

Appendix A. Extended comparison with experimental data and validation of the H_2/O_2 kinetic scheme

The updated mechanism was systematically compared against a wide range of experimental data (Table 1), including laminar flame speed, shock tube ignition delay time, flow reactors and burner-stabilized flames. Some of these results are reported in this paper as well as in Frassoldati et al. [21].

Mueller et al. [5] measured H_2, O_2, N_2 in an adiabatic flow reactor at pressures ranging from 0.3 to 15.7 atm and temperatures from 880 to 935 K. The adiabatic assumption and *time shifting* are used to take into account the non-ideal mixing at the inlet, as suggested by Mueller et al. [5] and Ó Conaire et al. [3].

Fig. A1 shows the good match obtained between measurements and modeling. At 3.44 atm, the system exhibits an induction period followed by rapid chain-explosive oxidation, while at higher pressure the H_2 consumption occurs in a slow and stable process. Again, as shown by the sensitivity analysis, the predicted results are largely sensitive to the competition between the $H + O_2 + [M] = HO_2 + [M]$ and $H + O_2 = OH + O$ reactions. Especially, at about 3 atm the recombination reaction exhibits very large sensitivity.

Because of its practical importance, the induction time in hydrogen–air systems is an active research topic involving both theoretical and experimental studies. In fact, experiments in shock tubes most closely represent the type of conditions associated with detonations and provide the measurement of the chemical induction time of the shocked mixture. Depending on the experimental technique, different definitions of the experimental induction time definitions exist which are usually associated with an initial rise (or maxima) in signals including pressure, radiation absorption, or radiation emission from a chemical species. Results from many of these measurements are used in this paragraph to test the predictive capabilities of the kinetic mechanism presented in Table 1.

Shock tube induction time data were compiled from the literature and accurately catalogued by Schultz and Shepherd [36] for hydrogen, ethylene and propane. They also discuss the aspects complicating the measurements which are the source of the uncertainties in the experimental data.

The revised thermodynamic properties of HO_2 influenced the results slightly reducing the ignition delay times in the range 950–1050 K.

Fig. A2 shows the good agreement between experimental measurements and model predictions for the ignition delay times in shock tube devices [72,74].

In the experiments of Schott and Kinsey [72] at 1 atm and Skinner and Ringrose [76] the ignition delays below 1200 K correspond to the time of maximum [OH], while above 1200 K to the time at which $[OH] = 10^{-6}\,mol/dm^3$. The experimental result is expressed as the ignition delay time multiplied by $[O_2]$.

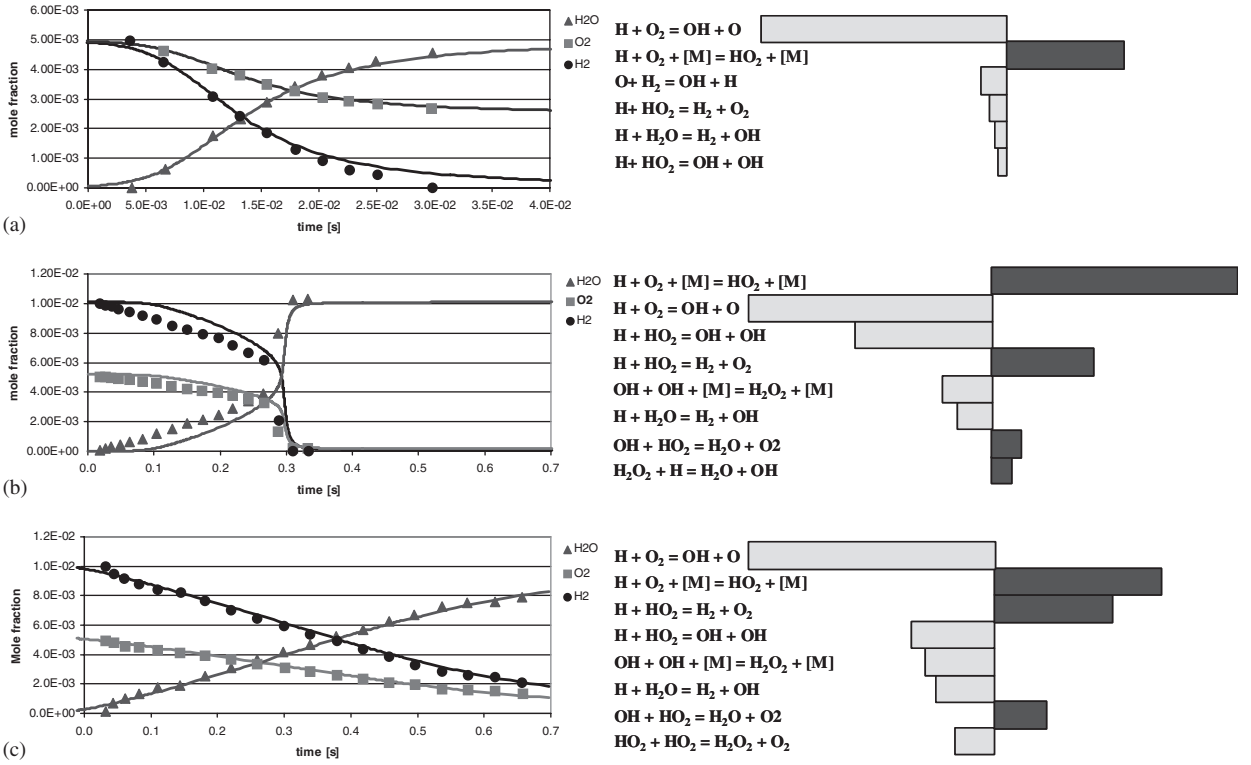

Fig. A1. Species profiles in a flow reactor and maximum sensitivity coefficients for $[H_2]$. Symbols are experimental data [5] and lines model predictions. Initial conditions: $H_2 = 1.01\%$, $O_2 = 0.52\%$, balance N_2. Dark bars correspond to positive sensitivity coefficients for $[H_2]$: (a) $P = 0.3$ atm, $T_{in} = 880$ K; (b) $P = 3.44$ atm, $T_{in} = 933$ K; (c) $P = 6.0$ atm, $T_{in} = 934$ K.

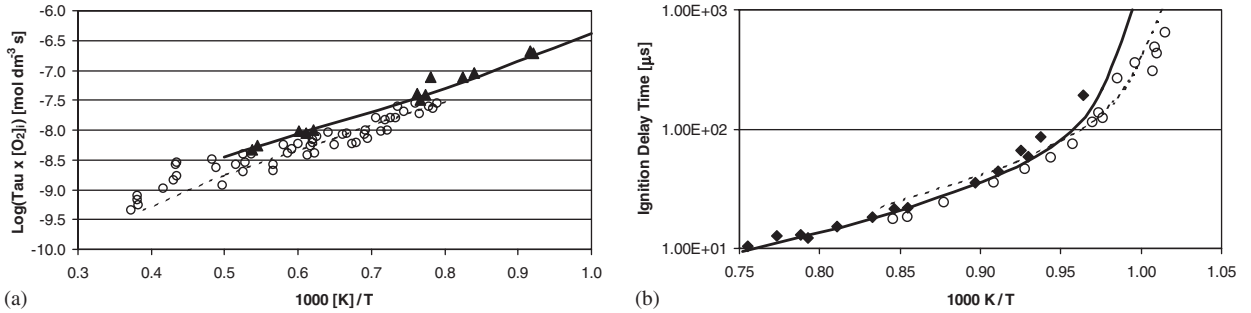

Fig. A2. (a) Comparison between predicted ignition delay times and experimental data [72] at 1 atm. Circles and dotted line: 4% H_2, 2% O_2, balance Ar. Triangles and continuous line: 1% H_2, 2% O_2, balance Ar. Criterion: maximum change of OH concentration. (b) Ignition delay times of $H_2/O_2/N_2$ mixture (29.59% H_2, 14.79% O_2, balance N_2). Circles and dotted line: experimental data [73] at 2 atm. Diamonds and continuous line: experimental data [74] at 2.5 atm.

Schott and Kinsey [72] studied diluted stoichiometric H_2–O_2 mixtures in Ar in a very wide range of temperatures, while Bhaskaran et al. [74] studied the ignition delay times at 2.5 atm and in the temperature range 1030–1330 K.

The ignition delay times measured by Hidaka et al. [75] and Skinner and Ringrose [76] are compared with model predictions in Fig. A3. The overall agreement is satisfactory. With respect to the mechanism of Ó Conaire et al. [3], the model predictions are slightly improved when considering the measurements at 1 atm (Fig. A3b) but a modest underestimation is obtained at 3 bar (Fig. A3a).

The mechanism is also in good agreement with the results of Fujimoto and Suzuki [77] although is too slow at temperatures below 950 K, as shown in Fig. A4a.

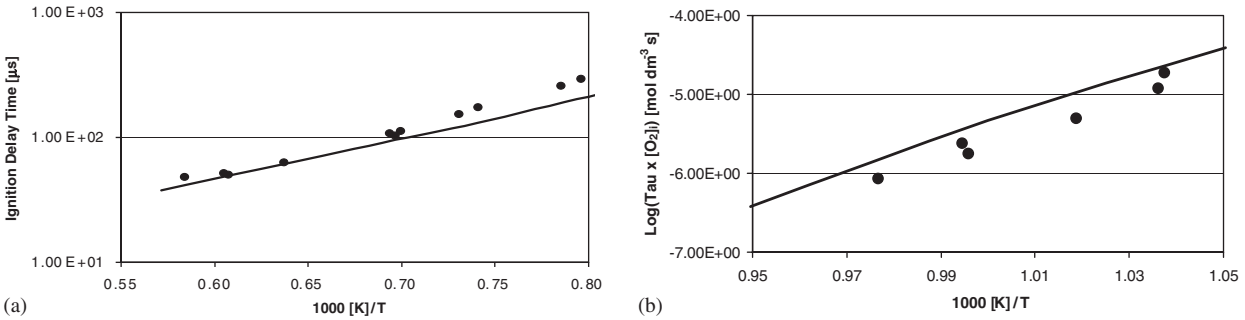

Fig. A3. (a) Comparison between predicted ignition delay times and experimental data [75] at 3 bar. 1% H_2, 1% O_2, balance Ar. (b) Comparison between predicted ignition delay times and experimental data [76] at 1 atm. 8% H_2, 2% O_2, balance Ar. Criterion: maximum OH concentration (both in experiment and calculations).

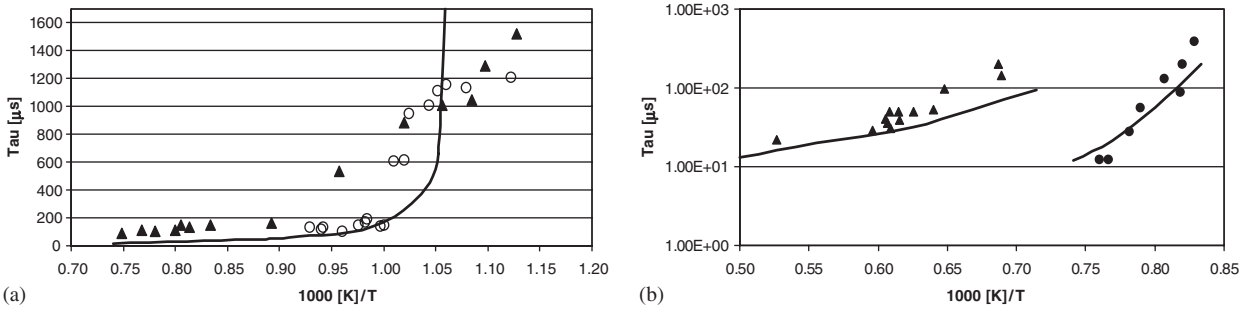

Fig. A4. (a) Comparison between predicted ignition delay times and experimental data [77] for stoichiometric H_2/air at 1 atm. Circles: pressure increase, triangles: light emission. (b) Ignition delay times for stoichiometric H_2/O_2/Ar mixture [78]. Circles: 2% H_2 at 33 atm: triangles: 0.1% H_2 at 64 atm; balance Ar. Lines represent model predictions.

The high pressure measurements of Petersen [78] are shown in Fig. A4b. The agreement is very satisfactory at 33 atm; however, the model slightly underestimates the ignition times at 64 atm.

The good agreement between measurements and model predictions obtained at sufficiently high temperatures reflects the good knowledge of the rate parameters for the chain-branching steps, especially $H + O_2 = OH + O$, which are known with good accuracy as already pointed out by Del Alamo et al. [1]. More challenging is the prediction of the induction time at lower temperatures, as crossover temperature is approached. Crossover is defined as the temperature at which the rates of chain-branching and termination reactions are equal [1]. The major chain-branching step is $H + O_2 = OH + O$ while the principal chain-breaking step is $H + O_2 + M = HO_2 + M$. The rate parameters for this reaction and particularly its third-body chaperon efficiencies are known with lower accuracy. As a consequence, kinetic mechanisms having different crossover temperature show large differences in predictions of ignition characteristics as described in detail by Del Alamo et al. [1].

The influence of steam concentration on the ignition delay times of H_2–air–steam mixtures was recently investigated by Wang et al. [37] behind the reflected shock wave. This study showed a strong dependence of the self-ignition characteristics on the steam concentration and temperature. Theoretical predictions were performed with the kinetic mechanism by means of a shock tube mathematical model and using the composition, pressure, temperature as those behind the reflected shock waves experimentally studied. The kinetic rate of the $H + O_2 + [M] = HO_2 + [M]$ third-body reaction and in particular the efficiency of H_2O are very important for this study with steam addition. The results (see the paper) confirm the role of the competition between chain branching and chin terminating reactions. The good agreement supports the kinetic parameters used in the present mechanism. It is interesting to observe that

Ó Conaire et al. [3] significantly improved their model predictions by adopting a third-body efficiency of 1.3 for H_2 in the $H + O_2 + [M] = HO_2 + [M]$ reaction, whereas Mueller et al. [5] adopted the same value used in the present study.

We do not include a separate rate expression for this reaction when the third-body is Ar or He as suggested by Mueller et al. [5], Li et al. [4], Konnov [33] and GRI 2.11 and 3.0 [34] for this and other reactions. In the present mechanism we use a value of H_2O third-body efficiency relative to Ar of 22.5, which is similar to the ones used by Ó Conaire et al. [3] 21, Del Alamo et al. [1] 24, and consistent with the indication of Hanson et al. [91] 17.8.

The results also show that the measured ignition delay times can be predicted quite well in the high temperature range but are overpredicted at low temperatures. These results are consistent with model predictions of Ó Conaire et al. [3] and Wang et al. [37] that obtained similar results using different kinetic mechanisms. The same deviation is not present for the other test cases presented in this section (Figs. A2–A4).

Vandooren and Bian [79] measured species concentrations in a premixed burner at equivalence ratio $\Phi = 1.91$ and low pressure. The predicted profiles well agree with experimental measurements (Fig. A5). Computations were performed using the experimental temperature profile.

Burning velocities in flames of $H_2/CO/CO_2$ and air were measured by Konnov et al. [80] and experimental results are shown in Fig. A6a. Two series of symbols represent day-to-day repeatability. The modeling of the adiabatic burning velocities at 298 K is in good agreement with experimental determinations.

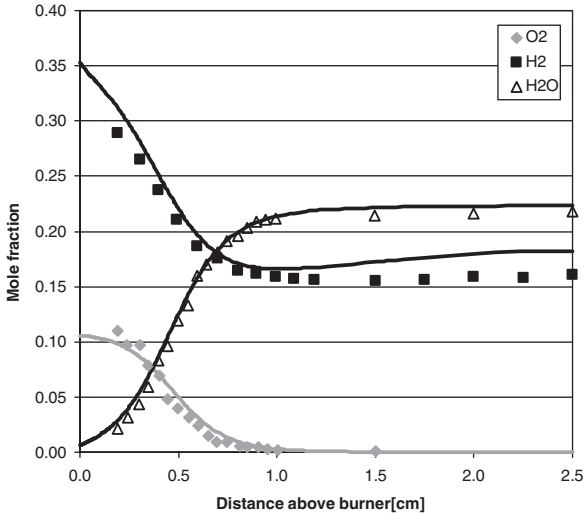

Fig. A5. Species profiles in a burner-stabilized flame at low pressure (35.5 torr). Initial conditions $H_2 = 39.7\%$, $O_2 = 10.3\%$, balance Ar. Symbols: experimental data [79].

The comparison with experimental measurements collected at 10 mm from the burner surface confirms the satisfactory agreement obtained in Fig. A6a. The sensitivity analysis reported in Fig. A7a illustrates the reactions which mostly affect the burning velocity. As expected the reaction between CO and OH is very important but the chemistry of the hydrogen/oxygen subset is also relevant. Similar results are shown in Fig. A7b for the pure H_2/air flame. The analysis confirms the effect on flame velocity of the recombination reaction between H and OH, as previously discussed.

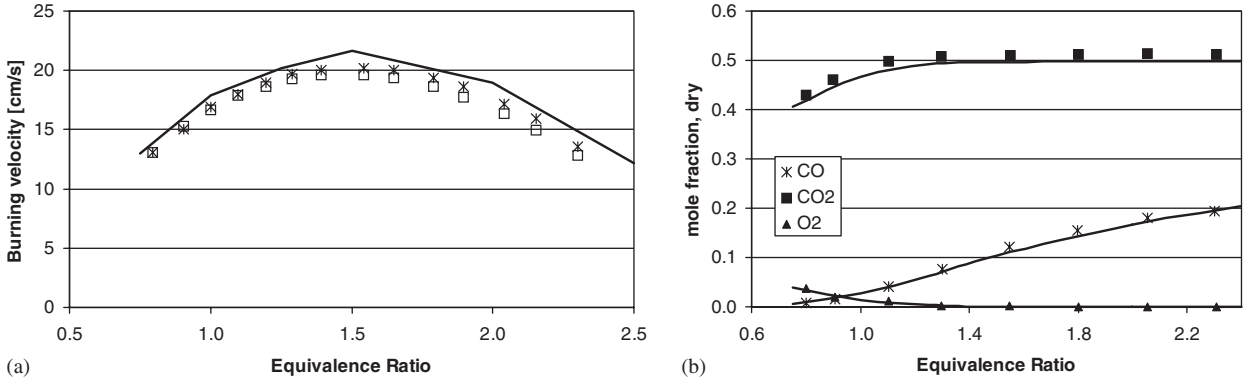

Fig. A6. (a) Adiabatic burning velocities in flames of $H_2/CO/CO_2$ and air ($H_2 = 5.05\%$, $CO = 44.75\%$, $CO_2 = 50.2\%$ in air at 298 K). Two series of symbols represent different series of experimental measurements [80]; solid line, modeling. (b) CO, CO_2 and O_2 at 10 mm from the burner as a function of equivalence ratio. Symbols: experimental measurements [80], solid lines: modeling.

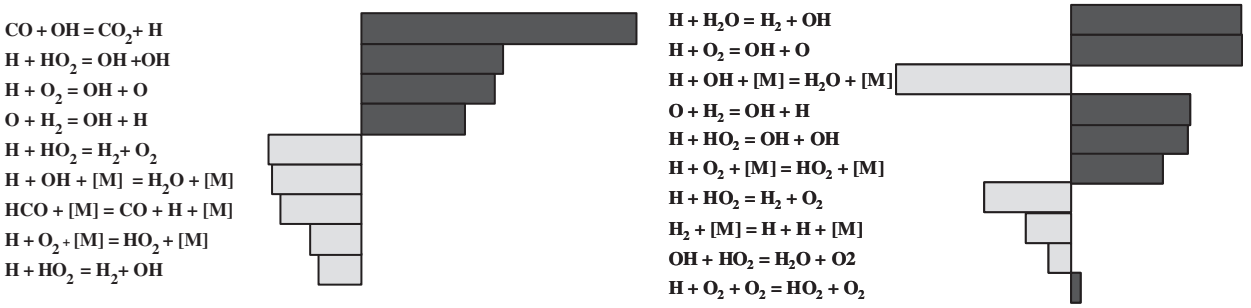

Fig. A7. Sensitivity coefficients for burning velocity: (a) flame of Fig. 6 at $\Phi = 2.0$, (b) H_2/air flame at $\Phi = 1.5$. Dark bars correspond to positive sensitivity coefficients.

References

[1] Del Alamo G, Williams FA, Sanchez L. Combust Sci Technol 2004;176:1599–626.

[2] Miller JA, Pilling MJ, Troe J. Proc Combust Inst 2005;30:43.

[3] Ó Conaire M, Curran HJ, Simmie JM, Pitz WJ, Westbrook KJ. Int J Chem Kinet 2004;36(11):603.

[4] Li J, Zhao Z, Kazakov A, Dryer FL. Int J Chem Kinet 2004;36(10):566.

[5] Mueller MA, Yetter RA, Dryer FL. Int J Chem Kinet 1999; 31:113.

[6] Ströhle J, Myhrvold T. Proceedings of the European combustion meeting, paper 7; 2005.

[7] Athens L, Claxton M, Waibel RT. Effect of fuel composition on emissions from ultra low NO_x burners. American flame research committee, Fall international symposium; 1995, ⟨http://www.johnzink.com/products/burners/pdfs/tp_effect_fuel_comp.pdf⟩.

[8] Faravelli T, Frassoldati A, Ranzi E. Combust Flame 2003; 132:188.

[9] Frassoldati A, Faravelli T, Ranzi E. Combust Flame 2003; 135:97.

[10] Kee RJ, Grcar JF, Smooke MD, Miller JA. A fortran program for modeling steady laminar 1-D premixed flames. Report SAND85-8240, Sandia National Laboratories; 1985.

[11] Lutz AE, Kee RJ, Grcar JF, Rupley FM. OPPDIF: a fortran program for computing opposed flow diffusion flames. Sandia Report, SAND96-8243; 1997.

[12] Kee RJ, Dixon-Lewis G, Warnatz J, Coltrin ME, Miller JA. Sandia Report, SAND86-8246, Sandia National Laboratories, Albuquerque, NM; 1986.

[13] Buzzi Ferraris G, Manca D. Comp Chem Eng 1998;22(11): 1595.

[14] Semenov NN. Acta Physicochim URSS 1945;20:291–302.

[15] Kee RJ, Rupley F, Miller JA. The Chemkin thermodynamic data base. Report SAND89-8008, Sandia National Laboratories, Livermore; 1989.

[16] Ruscic B, Wagner AF, Harding LB, Asher RL, Feller D, Dixon DA. et al. J Phys Chem A 2002;106:2727.

[17] Herbon JT, Hanson RK, Golden DM, Bowman CT. Proc Combust Inst 2002;29:1201–8.

[18] Hills AJ, Howard CJ. J Chem Phys 1984;81:4458–65.

[19] Ramond TM, Blanksby SJ, Kato S, Bierbaum VM, Davico GE, Schwartz RL. et al. J Phys Chem A 2002;106:9641–7.

[20] Marinov N, Westbrook CK, Pitz WJ. Detailed and global chemical kinetics model for hydrogen. In: Chan SH., , editor. Transport phenomena in combustion, vol. 1. Washington, DC: Talyor and Francis; 1996. (UCRL-JC-120677).

[21] Frassoldati A, Ranzi E, Faravelli T. Twenty eighth meeting of the Italian section of the combustion institute, combustion and urban areas. 4–7 July, Naples, Italy; 2005.

[22] Frassoldati A, Buzzi Ferraris G, Faravelli T, Pierucci S, Ranzi E. Second international conference on hydrogen era, chemical engineering transactions, vol. 8; 2005. p. 245. H2www@Sicily Conference, 16–19 October, Mondello Bay, Palermo; 2005.

[23] Ranzi E, Frassoldati A, Granata S, Faravelli T. Ind Eng Chem Res 2005;44(14):5170–83.

[24] Davis SG, Joshi AV, Wang H, Egolfopulos F. Proc Combust Inst 2005;30:1283.

[25] Saxena P, Williams FA. Combust Flame; 2005, in press.

[26] Troe J. Proc Combust Inst 2000;28:1463–9.

[27] Lewis B, Von Elbe G. Combustion, flames and explosions of gases. Cambridge: Cambridge University Press; 1938.

[28] Maas U, Warnatz J. Combust Flame 1988;74:53.

[29] Hinshelwood CN, Moelwyn-Hughes EA. Proc Roy Soc London Ser A 1932;138:311.

[30] Von Elbe G, Lewis B. J Chem Phys 1942;10:366.

[31] Heiple HR, Lewis B. J Chem Phys 1941;9:584.

[32] Egerton AC, Warren DR. Proc Roy Soc Ser A 1951;204:465.

[33] Konnov AA. Detailed reaction mechanism for small hydrocarbons combustion. Release 0.5 ⟨http://homepages.vub.ac.be/~akonnov/⟩; 2000.

[34] Bowman CT, Hanson RK, Davidson DF, Gardiner Jr. WC. Lissianski V, Smith GP, et al. GRI-Mech. ⟨http://www.me.berkeley.edu/gri_mech/⟩.

[35] Skreiberg O, Kilpinen P, Glarborg P. Combust Flame 2004; 136:501–18.

[36] Schultz E, Shepherd J. Validation of detailed reaction mechanisms for detonation simulation. Explosion Dynamics Laboratory Report FM99-5, California Institute of Technology; 2000, ⟨http://www.galcit.caltech.edu/EDL/publications/reprints/galcit_fm99-5.pdf⟩.

[37] Wang BL, Olivier H, Grönig H. Combust Flame 2003;133: 93–106.

[38] Aung KT, Hassan MI, Faeth GM. Combust Flame 1997;109:1.

[39] Dowdy DR, Smith DB, Taylor SC. Proc Combust Inst 1990;23:325.

[40] Wu CK, Law CK. Proc Combust Inst 1984;20:1941.

[41] Takahashi F, Mizomoto M, Ikai S. Alternative Energy Sources III 1983;5:447.
[42] Iijima T, Takeno T. Combust Flame 1986;65:35.
[43] Tse SD, Zhu DL, Law CK. Proc Combust Inst 2000;28:1793.
[44] Kwon OC, Faeth GM. Combust Flame 2001;124:590.
[45] Seiser R, Seshadri K. Proc Combust Inst 2005;30.
[46] Rørtveit GJ, Hustad JE, Li SC, Williams FA. Combust Flame 2002;130:48.
[47] Park J, Kim SC, Keel SI, Noh DS, Oh CB, Chung D. Int J Energy Res 2004;28:1075–88.
[48] Bozzelli JW, Dean AM. Int J Chem Kinet 1995;27:1097.
[49] Konnov AA. Combust Flame 2003;134:421.
[50] Harrington JE, Smith GP, Berg PA, Noble AR, Jeffries JB, Crosley DR. Proc Combust Inst 1996;26:2133.
[51] Homer JB, Sutton MM. Combust Flame 1973;20:71.
[52] Xie L, Hayashi S, Hirose K. Proc Combust Inst 1996;26:2155.
[53] Laster WR, Sojka PE. J Propul Power 1989;5(4):385–90.
[54] Slack MW, Grillo AR. Combust Flame 1978;31:275–83.
[55] Borisov AA, Skachkov GI. Kinetika i Kataliz 1972;13(1):42–7.
[56] Konnov AA. ⟨http://homepages.vub.ac.be/∼akonnov/science/mechanism/test.html⟩; 2005.
[57] Rohrig M, Petersen EL, Davidson DF, Hanson RK. Int J Chem Kinet 1996;28:599.
[58] Li SC, Williams FA. Combust Flame 1999;118:399–414.
[59] Johnsson JE, Glarborg P, Dam-Johansen K. Proc Combust Inst. 1992;24:917.
[60] Bendtsen AB, Glarborg P, Dam-Johansen K. Combust Sci Technol 2000;151:31–71.
[61] Brown MJ, Smith DB. Proc Combust Inst 1994;25:1011.
[62] Glarborg P, Jensen AD, Johnson JE. Prog Energy Combust Sci 2003;29:89–113.
[63] Sausa RC, Singh G, Lemire W, Anderson WR. Proc Combust Inst 1996;26:1043.
[64] Dagaut P, Lecomte F, Chevailler S, Cathonnet M. Combust Sci Technol 1998;139:329.
[65] Klaus P, Warnatz J. ⟨http://reaflow.iwr.uni-heidelberg.de/∼ftp/reaflow/mechanism_for_export/Mech97.C1_C2_NO+thermodynamics⟩; 1997.
[66] Hasegawa T, Sato M. Combust Flame 1998;114:246.
[67] Fujii N, Miyama H, Koshi M, Asaba T. Proc Combust Inst 1981;18:873–83.
[68] Shin KS, Bae GT, Shim SB, Ryu S-O. J Korean Chem Soc 2001;45(2):111.
[69] Cohen L. Fuel 1955;34:123.
[70] Murray RC, Hall AR. Trans Faraday Soc 1951;47:743.
[71] Zakaznov VF, Kursheva LA. Zh Prikl Khim 1980;53:1865.
[72] Schott GL, Kinsey JL. J Chem Phys 1958;29:1177.
[73] Slack MW. Combust Flame 1977;28:241.
[74] Bhaskaran KA, Gupta MC, Just Th Combust Flame 1973;21:45.
[75] Hidaka Y, Sato K, Henmi Y, Tanaka H, Inami K. Combust Flame 1999;118:340–58.
[76] Skinner GB, Ringrose GH. J Chem Phys 1965;42:2190–2.
[77] Fujimoto S, Suzuki M. Memoirs Defense Academy Japan 1967;VII(3):1037–46.
[78] Petersen EL, Davidson DF, Röhrig M, Hanson RK. 20th International symposium shock waves; 1996. p. 941–6.
[79] Vandooren J, Bian J. Proc Combust Inst 1990;23:341.
[80] Konnov AA, Dyakov IV, De Ruyck J. Proc Combust Inst 2002;29:2171–7.
[81] Baulch DL, Drysdale DD, Horne DG. An assessment of rate data for high-temperature systems. Proc Combust Inst 1973;14:107–18.
[82] NIST Chemical Kinetics Database. ⟨http://kinetics.nist.gov/index.php⟩.
[83] Davidson DF, Petersen EL, Rohrig M, Hanson RK, Bowman CT. Proc Combust Inst 1996;26:481–8.
[84] Ranzi E, Sogaro A, Gaffuri P, Pennati G, Faravelli T. Combust Sci Tech 1994;96(4–6):279–325.
[85] Lloyd AC. Int J Chem Kinet 1974;6:169–228.
[86] Baulch DL, Cobos CJ, Cox RA, Frank P, Hayman G, Just Th et al. J Phys Chem Ref Data 1994;23:847–1033.
[87] Baulch DL, Cobos CJ, Cox RA, Esser C, Frank P, Just Th et al. J Phys Chem Ref Data 1992;21:411–29.
[88] Tsang W, Hampson RF. J Phys Chem Ref Data 1986;15:1087–279.
[89] Sehested J, Mogelberg T, Fagerstrom K, Mahmoud G, Wallington TJ. Int J Chem Kinet 1997;29:673–82.
[90] Brouwer L, Cobos CJ, Troe J, Dubal H-R, Crim FF. J Chem Phys 1987;86:6171.
[91] Hanson RK, Golden DM, Bowman CT, Davidson DF, Bates RW. First joint meeting of the US sections of the combustion institute. The George Washington University, Washington DC, March 14–17; 1999.